OATAO
Open Archive Toulouse Archive Ouverte

Open Archive Toulouse Archive Ouverte (OATAO)

OATAO is an open access repository that collects the work of Toulouse researchers and makes it freely available over the web where possible.

Any correspondence concerning this service should be sent to the repository administrator: staff-oatao@listes.diff.inp-toulouse.fr

On the existence and evolution of a spanwise vortex in laminar shallow water dipoles

J. Albagnac, L. Lacaze, P. Brancher, and O. Eiff

Related Articles

Conditional vorticity budget of coherent and incoherent flow contributions in fully developed homogeneous isotropic turbulence
Phys. Fluids 24, 035108 (2012)

Flow visualization of a vortex ring interaction with porous surfaces
Phys. Fluids 24, 037103 (2012)

Boundary layer turbulence in transitional and developed states
Phys. Fluids 24, 035105 (2012)

Energy exchange between a vortex ring and an ionic polymer metal composite
Appl. Phys. Lett. 100, 114102 (2012)

Strain-vorticity induced secondary motion in shallow flows
Phys. Fluids 24, 023601 (2012)

Additional information on Phys. Fluids

On the existence and evolution of a spanwise vortex in laminar shallow water dipoles

J. Albagnac,[1,2] L. Lacaze,[1,2] P. Brancher,[1,2] and O. Eiff[1,2]

[1]*Université de Toulouse, INPT, UPS, Institut de Mécanique des Fluides de Toulouse, Allée Camille Soula, F-31400 Toulouse, France*
[2]*CNRS, Institut de Mécanique des Fluides de Toulouse, F-31400 Toulouse, France*

The present work investigates the existence and evolution of a spanwise vortex at the front of shallow dipolar vortices. The vortex dipoles are experimentally generated using a double flap apparatus. Particle image velocimetry measurements are performed in a horizontal plane and in the vertical symmetry plane of the flow. The dynamics of such vortical structures is investigated through a parametric study in which both the Reynolds number $Re = U_0 D_0/\nu \in [90, 470]$ and the aspect ratio $\alpha = h/D_0 \in [0.075, 0.7]$, associated with the shallowness of the flow, are varied, where U_0 is the initial velocity of the vortex dipole, D_0 is the initial diameter, h is the water depth, and ν is the kinematic viscosity of the fluid. The present experiments confirm the numerical results obtained in a companion paper by Duran-Matute *et al.* [Phys. Fluids **22**, 116606 (2010)], namely that the flow remains quasi parallel with negligible vertical motions below a critical value of the parameter $\alpha^2 Re$. By contrast, for large values of $\alpha^2 Re$ and $\alpha \lesssim 0.6$, a three-dimensional regime is observed in the shape of an intense spanwise vortex generated at the front of the dipole. The present study reveals that the early-time motion and dynamics of the spanwise vortex do not scale on the unique parameter $\alpha^2 Re$ but is strongly influenced by both the aspect ratio and the Reynolds number. A mechanism for the generation of the spanwise vortex is proposed. For $\alpha \gtrsim 0.6$, a third regime is observed, where the spanwise vortex is replaced by a vorticity tongue. © *2011 American Institute of Physics*. [doi:10.1063/1.3611419]

I. INTRODUCTION

Vortex dipoles are pairs of counter-rotating vortices in close interaction observed in various coastal flows such as rip currents[1] or close to the outflow after estuaries.[2] These vortical structures are associated with sediment transport and pollutant dispersion. For example, Ahlnas *et al.*[3] have used satellite images of the oceanic surface to show the existence of upwelling motions in vortex dipoles, which were observed to put sediment into suspension from the seabed into the core of the dipole vortices.

While the dynamics of vortex dipoles under continuous stable stratification in the atmospheric and oceanic context has received considerable attention in the last couple decades,[4–8] studies of dipoles in a shallow water situation are more recent.[9,10] Not surprisingly, since vertical motions are inhibited in both cases, the long-term dynamics are quasi two-dimensional (Q2D). Also, in both cases, an initially three-dimensional (3D) injection of turbulent fluid leads to the formation of vortex dipoles,[4,11] in the shallow water situation, however, only when sufficiently confined.[12]

Yet, for shallow vortex flows, recent studies have revealed a more complex picture than Q2D dynamics.[11,13,14] For example, Lin *et al.*[14] have analyzed the 3D structure of vortex dipoles generated by a piston-nozzle arrangement in a shallow water configuration. Their experiments revealed a hierarchy of secondary vortices wrapping around the core of the primary vortices composing the dipole. More significantly, they also observed a dominant recurrent vortex struc-

ture whose vorticity is not vertical but horizontal and with up to twice the peak value of the primary vortices. Similarly, Sous *et al.*,[11,12] in their study of vortex dipoles resulting from the decay of an impulsive turbulent jet in a shallow layer, observed a transverse circulation at the front of the dipole. More recently, Akkermans *et al.*[15–17] performed experimental and numerical studies on shallow vortex dipoles generated by electromagnetic forcing. While their work focused on the vertical motions in the vortex cores of the dipole itself, the presence of a frontal transverse circulation is also mentioned.

In order to analyze the basic physical mechanisms at the origin of the observed secondary circulation deviating from Q2D dynamics, Lacaze *et al.*[18] investigated the 3D dynamics of vortex dipoles at low Reynolds numbers. In their study, velocity measurements in the vertical symmetry plane confirmed the presence of a strong spanwise vortex at the front of the dipole and this at low Reynolds numbers. They thus suggested that the spanwise vortex is a generic feature of shallow vortex dipoles for a large range of Reynolds numbers. Yet, the conditions of generation and existence, as well as the motion and dynamics of the spanwise vortex, have not yet been examined, motivating the present experimental parametric study.

The specific objectives of the present study are twofold. First, they are to examine experimentally the conditions of deviation from Q2D dynamics and more particularly to delimit the regime for the formation of the secondary transverse vortex appearing at the front of the dipole. Second, they

are to give a detailed description and analysis of the influence of the two basic control parameters, the Reynolds number Re and the aspect ratio α, on the time development and dynamics of the spanwise vortex in relation to the primary dipolar vortex structure. Emphasis will be put on generating an initially Q2D vortex dipole in order to ascertain that the origin of the three-dimensionalization lies in the quasi-two dimensional nature of the flow. The forcing will thus be two-dimensional as in Lacaze *et al.*[18]

The present experimental study also inspired a companion numerical parametric study presented in Duran-Matute *et al.*,[19] hereafter referred to as DMA. This companion work also includes some experiments for comparison issued, however, from a vortex generation forcing which is vertically dependent and therefore different from the one presented here. The focus of the DMA study was to provide a numerical-simulation based identification of the different flow regimes and to examine the strength of the secondary vertical motions within the global hydrodynamic structure rather than the specific dynamics of the spanwise vortex. The DMA results show that the relative strength of these secondary vertical motions has qualitatively the same scaling properties as in a shallow axisymmetric monopolar vortex in a viscosity-dominated regime.[20] Moreover, for small values of the parameter $\alpha^2 Re$, a parameter whose role in axisymmetric swirl flows had been shown by Duran-Matute *et al.*,[20] a viscosity-dominated Q2D regime exists, whereas above a critical value, a persistent spanwise vortex is observed. These regime identifications will be compared with the experimental results obtained here.

The experimental set-up and the associated measurement techniques are described in Sec. II which includes the presentation of the parametric study. The description of the time evolution of the horizontal and vertical structures of a shallow vortex dipole in the presence of a spanwise vortex is presented in Sec. III. Then, the influence of the shallowness and Reynolds number on the existence and time evolution of the spanwise vortex is analyzed in Secs. IV and V. Finally, a summary of the results and the perspectives of this study are given in Sec. VI.

II. EXPERIMENTAL SET-UP

A. Vortex dipole generator

The experiments are performed in a 2 m long, 1 m wide, and 0.7 m deep tank filled with a layer of water of depth $h \in [0.5, 4.5]$ cm, initially at rest (Fig. 1). Vortex dipoles are generated by the device used by Billant and Chomaz[21] and Lacaze *et al.*[18] A pair of vertical flaps initially parallel to each other are put into rotation toward each other along a vertical axis with linearly decreasing angular velocity during a closing time T_c. Shear layers are generated on the flaps which roll up at the trailing edges to form two counter-rotating starting vortices. The resulting vortex dipole then propagates away by mutual induction. The flap separation at the base $d = 6.5$ cm and initial closing angle $\beta_0 = 14°$ are chosen in order to minimize the influence of the stopping vortices created at the end of the flaps motion (see Ref. 21 for details).
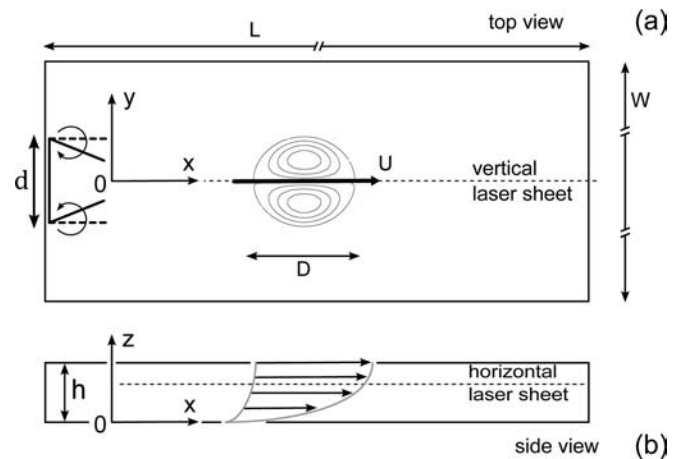

FIG. 1. Experimental set-up: (a) top and (b) side views. The sketch is not to scale.

Such an experimental set-up generates laminar, symmetric, and reproducible vortex dipoles.

In the following, x, y, and z, respectively, denote the streamwise, spanwise, and vertical directions. The origins of the x, y, and z axes are, respectively, located at the flaps' trailing edge, at the vertical symmetry plane and at the tank bottom (see Fig. 1). The initial time $t = 0$ s corresponds to the end of the flap closing.

B. Measurement techniques

Particle image velocimetry (PIV) measurements are performed in a horizontal plane at $z = 2h/3$ and in the vertical symmetry plane $y = 0$ (see Fig. 1). The images are recorded during a 100-s interval beginning at the start of the flap closing. PIV measurements in the horizontal plane are performed with a single Nd-YAG 30 mJ pulsed laser and a 1280×1024 pixels 12-bit CCD camera. Two 1280×1024 pixels 12-bit CCD cameras positioned side by side coupled with a single Nd-YAG 30 mJ pulsed laser are used to perform the PIV measurements in the vertical symmetry plane. The fields recorded by the two cameras overlap allowing a single instantaneous field to be properly reconstructed. This yields the same horizontal extent as the horizontal PIV measurements while doubling the vertical resolution where the gradients are expected to be stronger.

The velocity fields are computed from pairs of consecutive images by a spatial correlation technique[22] with peak-locking reduction algorithms developed by Fincham and Delerce.[23]

C. Parametric study

Shallow vortex dipoles can be characterized by three dimensional parameters: the initial dipole diameter D_0, its initial propagation speed U_0, and the water depth h. The present experimental set-up controls the first two parameters via the distance d between the flaps, the flap closing time T_c, and the closing angle β_0 as follows.

Experimental observations show that the initial vortex dipole diameter D_0 depends very weakly on the water depth h and on the flap closing time T_c, at least in the range of
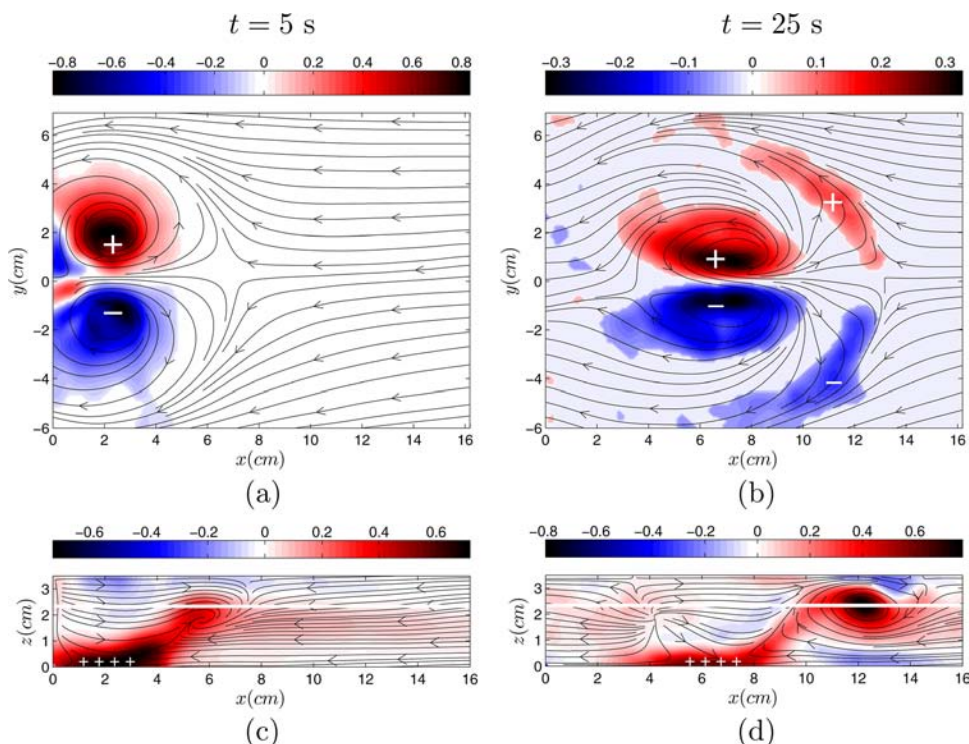
FIG. 2. (Color online) Time evolution of the vertical vorticity ω_z (s^{-1}) in the horizontal plane $z/h = 2/3$ (a) and (b) and of the horizontal vorticity ω_y (s^{-1}) in the vertical symmetry plane (c) and (d). The sectional streamlines (black solid lines) are computed in the reference frame moving with the dipole. $+$ and $-$ symbols indicate the sign of the different vorticity patterns. The white lines in (c) and (d) mark the position of the horizontal PIV plane at $z/h = 2/3$. $(Re, \alpha) = (290, 0.54)$.

parameters used for the present study. In particular, the initial vortex dipole diameter, defined as twice the distance between the vortex centers, varies between 6 cm and 7 cm around a mean value of $D_0 = 6.5$ cm which is found to match the distance d between the flaps. This mean initial diameter $D_0 (= d)$ will be used as the characteristic horizontal length scale in the following.

As in Billant and Chomaz,[21] for (deep) stratified dipoles [see their Fig. 4(a)], the initial dipole velocity U_0 is found to be inversely proportional to the closing time T_c for a given flap separation d and a given closing angle β_0. Specifically, the initial velocity of the shallow water dipole follows the law $U_0 \approx a/T_c$ cm s^{-1} with $a = 3.6$ cm. This law is the same as in Billant and Chomaz[21] with the same constant.

We define the Reynolds number of the dipole as $Re = U_0 D_0/\nu$ where ν is the kinematic viscosity. This definition is equivalent to $Re = ad/\nu T_c$ with the dimensional parameters of the experimental set-up. The second non-dimensional control parameter is the aspect ratio $\alpha = h/D_0$ between the water depth h and the initial dipole diameter D_0. The lower the aspect ratio α, the shallower the flow. Each experiment is therefore defined by the non-dimensional couple (Re, α), associated with the dimensional couple (T_c, h). In the present study, $T_c \in [5, 25]$ s and $h \in [0.5, 4.5]$ cm, yielding $Re \in [90, 470]$ and $\alpha \in [0.075, 0.7]$. These ranges have been chosen such as to explore the parameter space around the configuration of Lacaze *et al.*[18] where the spanwise vortex was observed, in order to investigate independently the influence of the Reynolds number and the aspect ratio on the existence and dynamics of the spanwise vortex.

III. TIME EVOLUTION OF THE 3D VORTEX DIPOLE

A. In the horizontal plane

Figures 2(a) and 2(b) show the vertical vorticity field ω_z in the horizontal plane at $z/h = 2/3$ for $Re = 290$ and $\alpha = 0.54$ at $t = 5$ s [Fig. 2(a)] and $t = 25$ s [Fig. 2(b)]. The solid black lines denote the sectional streamlines (equivalently referred to as flow lines) which are tangential to horizontal velocity components in the horizontal plane in the reference frame moving with the dipole.

In Fig. 2(a), the two vorticity patches correspond to the pair of counter-rotating primary vortices composing the dipole. The sectional streamlines reveal the classical structure of the velocity field of a vortex dipole, with a separatrix streamline separating the rotational part of the flow (the vortex dipole) from the (quasi) potential part. Within the dipole, the sectional streamlines spiral around two focal points indicating vertical motions within the primary vortex cores, as observed by Akkermans *et al.*[15,16] These vertical motions are induced by viscous layer suction as characterized by Satijn *et al.*[13] in the case of a confined and axisymmetric monopolar vortex. Topological constraints[24] impose the presence of two saddle points in a plane intersecting a vortex dipole. One of them is visible in the horizontal plane in Fig. 2(a): it is located at the dipole front and on the axis of symmetry of the dipole ($y = 0$). The other one is on the same axis at the rear but outside the measurement field. It is important to note that the saddle point at the front is associated with horizontal compression in the streamwise direction and stretching in the spanwise direction. The role of the latter on the three-dimensional dynamics will be discussed in Sec. V.

At $t = 25$ s [Fig. 2(b)], the primary vortices have propagated in the streamwise direction on a distance of order D_0. During this time, the horizontal shape of the vortex dipole has changed drastically: the primary vortices, which were initially almost circular, have become elliptical, and two opposite vorticity patches have appeared on each side at the front of the dipole. Such an evolution indicates a global modification of the flow structure, which has become more complex.

B. In the vertical plane

Figures 2(c) and 2(d) display iso-contours of spanwise vorticity ω_y and the associated sectional streamlines in the vertical plane $y = 0$ corresponding to the symmetry plane of the vortex dipole at the same time as in Figs. 2(a) and 2(b).

In Fig. 2(c), high levels of spanwise vorticity are observed close to the solid bottom. This spanwise vorticity is located at the same streamwise position as the primary vortices [see Fig. 2(a)] and is the signature of the viscous boundary layer induced by the propagation of the dipole over the solid bottom. Weaker spanwise vorticity is also observed above the boundary layer at the front of the dipole. The position of this weaker spanwise vorticity coincides with the region of horizontal stretching in the vicinity of the saddle point at the front of the dipole.

Figure 2(d) shows that the spanwise vorticity associated with the viscous boundary layer has decreased whereas the spanwise vorticity at the front of the dipole has increased above the maximum value in the boundary layer. The associated sectional streamlines now roll up around a focal point corresponding to an extremum of spanwise vorticity. This observation strongly suggests that the patch of vorticity corresponds to a spanwise vortex. The maximum vorticity of this vortex is stronger than that of the primary vortices [Figs. 2(b) and 2(d)], as observed by Lacaze *et al.*[18] and Duran-Matute *et al.*[19] As seen in Fig. 2(d), this vortex intersects the horizontal plane (white line at $z = 2h/3$) at the meeting point of the secondary vertical vorticity patches in the horizontal plane [Fig. 2(b)] that extend on each side of the axis of symmetry $y = 0$. The spanwise vortex in the vertical plane and the secondary vorticity patches in the horizontal plane are therefore correlated and part of the same vortical structure. Also, the sign of the secondary vorticity patches in the horizontal plane indicates that the vortex lines extending from the spanwise vortex in the symmetry plane tilt upwards toward the free surface while enveloping the front of the dipole.

IV. EFFECTS OF REYNOLDS NUMBER AND ASPECT RATIO

This section investigates the conditions under which the spanwise vortex is observed depending on the flow control parameters, i.e., the aspect ratio α and the Reynolds number Re. The flow is analyzed via the PIV measurements in the vertical symmetry plane.

A. Description of the different flow regimes

Three different flow regimes have been observed for the range of parameters examined $Re \in [90, 470]$ and $\alpha \in [0.075, 0.7]$. Typical iso-contours of spanwise vorticity ω_y and sectional streamlines in the vertical symmetry plane and in the reference frame moving with the dipole are shown in Figs. 3(a)–3(c) for the three regimes identified.

The flow displayed in Fig. 3(a) at $(Re, \alpha) = (235, 0.15)$ illustrates the first regime. In this regime, the spanwise vorhicity ω_y expands over the entire water depth and the sectional streamlines remain essentially horizontal and parallel. No spanwise vortex is observed. This flow regime will be referred to as the "quasi-parallel" regime.

For a larger aspect ratio α and similar Re, as shown in Fig. 3(b) for $(Re, \alpha) = (290, 0.38)$, the sectional streamlines roll up locally around the maximum of spanwise vorticity ω_y. This behavior, also observed in Fig. 2(d), is associated with the presence of a spanwise vortex, which can be objectively dissociated from the viscous boundary layer since two local maxima of spanwise vorticity co-exist, one being directly associated with the boundary layer and the other with the spanwise vortex. Moreover, the presence of this vortex is confirmed by the λ_2-criterion, as shown in the following (see Fig. 5). This flow regime will therefore be referred to as the "spanwise vortex" regime.

When the aspect ratio α is increased further at lower values of the Reynolds number Re, the vorticity field in the vertical symmetry plane does not present any localized maximum. A typical example is shown in Fig. 3(c) for $(Re, \alpha) = (120, 0.69)$. This regime is characterized by a tongue of monotonically decreasing spanwise vorticity extending up through the water layer, along the region of positive stretching at the front of the dipole. Contrary to the
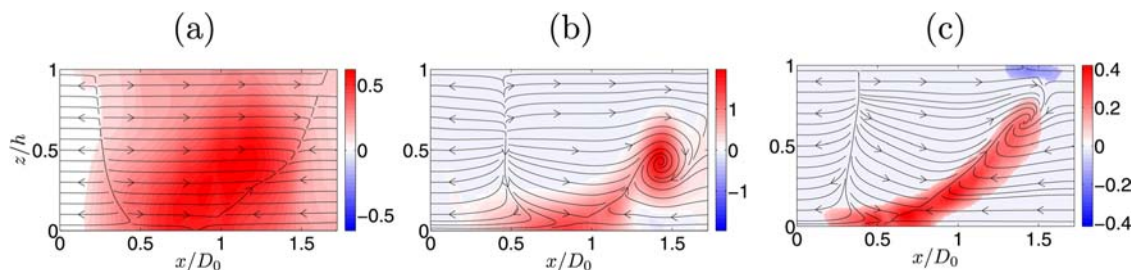
FIG. 3. (Color online) Spanwise vorticity fields ω_y (s^{-1}) in the vertical symmetry plane of the dipole for the three regimes observed in the present experiments. Black lines correspond to the sectional streamlines in the reference frame moving with the dipole. (a) $(Re, \alpha) = (235, 0.15)$ at $t = 13.5$ s, (b) $(Re, \alpha) = (290, 0.38)$ at $t = 12.2$ s, (c) $(Re, \alpha) = (120, 0.69)$ at $t = 14.3$ s. The horizontal and vertical axes are non-dimensionalized by the dipole diameter and the water depth, respectively.

previous regime, no vortex is identified by the λ_2-criterion in this case. This flow regime will be referred to as the "vorticity tongue" regime.

B. The flow regimes in the parameter space

The three flow regimes are identified in the parameter space (α, Re) in Fig. 4(a). It can be seen that the critical Reynolds number Re_c above which the spanwise vortex is observed depends on the aspect ratio α. This suggests that an alternative scaling might be more relevant when considering the conditions of existence of the spanwise vortex. As done classically in studies on Q2D vortex dipoles, the present Reynolds number has been defined as the ratio of the diffusion time D_0^2/ν based on the horizontal characteristic length-scale D_0 and the advection time D_0/U_0. Yet in the present case, it should be underlined that the spanwise vortex cannot exist if viscous diffusion in the vertical direction through the water layer is much stronger than inertia. This suggests a more relevant diffusion timescale h^2/ν based on the thickness of the fluid layer. With this new scaling, the competition between (vertical) diffusion and (horizontal) inertia is quantified by the ratio $(h^2/\nu)/(D_0/U_0) = \alpha^2 Re$. It is noteworthy that this parameter $\alpha^2 Re$ has been identified by the scaling analysis of Duran-Matute et al.[20] as the relevant control parameter associated with the generation of secondary vertical motions at the periphery of a single shallow vortex.

Figure 4(b) shows the different regimes identified in the present study but also extracted from previous observations[11,12,14–16,19] in the new parameter space (α, $\alpha^2 Re$). This rescaling allows one to identify a critical value $\alpha^2 Re \approx 6$ (dashed line) above which the spanwise vortex is observed. This value, which has been confirmed by the numerical simulations of DMA, does not depend on the aspect ratio α, at least if α is small enough ($\alpha \lesssim 0.6$). For larger α, when the flow is too deep to be considered shallow, the three-dimensional vortex dipole displays complex features induced by large depth effects, as exemplified by the vorticity tongue regime described in Sec. IV A.

A criterion for the existence of the spanwise vortex can be qualitatively derived as follows. Lacaze et al.[18] found the spanwise vortex radius a to be well evaluated from a balance between viscous diffusion and vortex stretching, as in the Burgers vortex model. This assumption leads to $a \approx \sqrt{\nu/\gamma}$, where $\gamma \approx U_0/D_0$ is of the order of magnitude of the spanwise stretching at the front of the dipole. A necessary condition for the existence of the spanwise vortex is that its diameter does not exceed the water depth h. This geometric constraint qualitatively corresponds to the condition $a < h$, which results in the criterion $\alpha^2 Re > 1$. This criterion underlines the relevance of the parameter $\alpha^2 Re$ and is in agreement with the experimental results of Fig. 4(b).

V. EVOLUTION AND DYNAMICS OF THE SPANWISE VORTEX

This section focuses on the regime in which the spanwise vortex exists. The objective is to analyze the generation of the spanwise vortex and then its time evolution by investigating the influence of the Reynolds number Re and the aspect ratio α. For this purpose, three particular cases are considered: (Re, α) = (290, 0.3) (case I), (290, 0.54) (case II), and (180, 0.54) (case III) [black filled circles in Figs. 4(a) and 4(b)]. The influence of the aspect ratio α will be quantified through the comparison of cases I and II. The influence of the Reynolds number Re will be quantified through the comparison of cases II and III.

A. Generation of the spanwise vortex

The time evolution of the spanwise vorticity field in the vertical symmetry plane of the vortex dipole is shown in Fig. 5 for case II ($\alpha = 0.54$, $Re = 290$). In this figure, solid lines correspond to the λ_2-criterion (see Ref. 25). The λ_2-
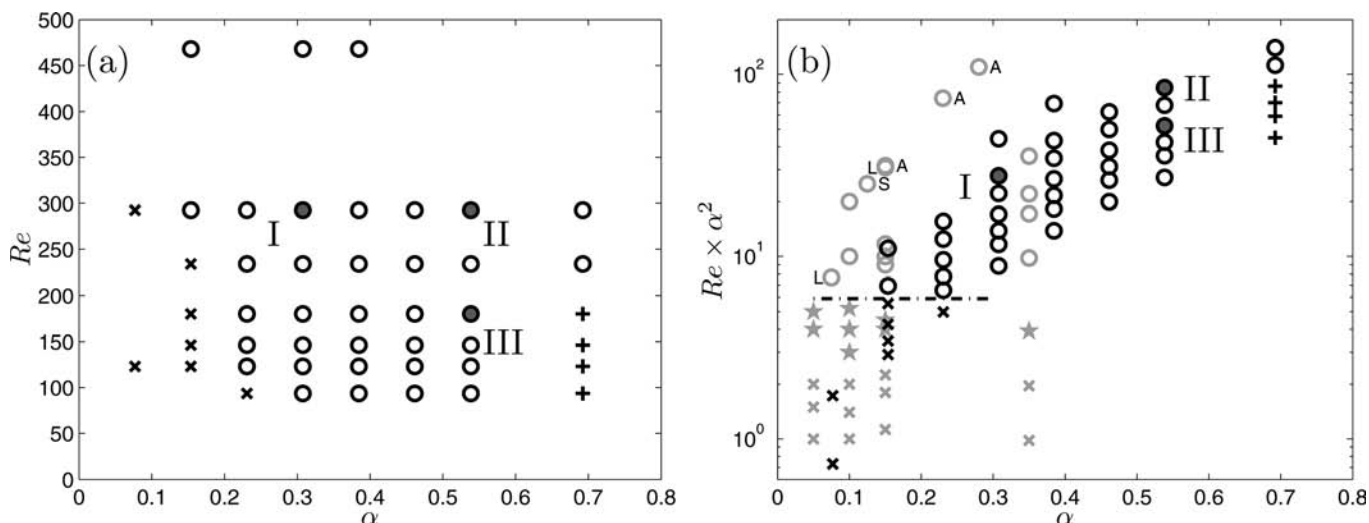
FIG. 4. The different regimes in the parameter space (α, Re) (a) and (α, $\alpha^2 Re$) (b). Quasi-parallel flow ($\times$), spanwise vortex ($\circ$), and vorticity tongue ($+$). The dashed line in (b) separates the quasi-parallel flow regime (with no spanwise vortex) from the regime characterized by the presence of a persistent spanwise vortex. Black filled circles correspond to the cases detailed in Sec. V. Grey symbols are estimations of previous results by Duran-Matute et al.,[19] Lin et al.[14] (L), Akkermans et al.[15,16] (A), and Sous et al.[11,12] (S). Grey stars correspond to the transitional regime of Duran-Matute et al.,[19] where the spanwise vortex has been transiently observed in numerical simulations.
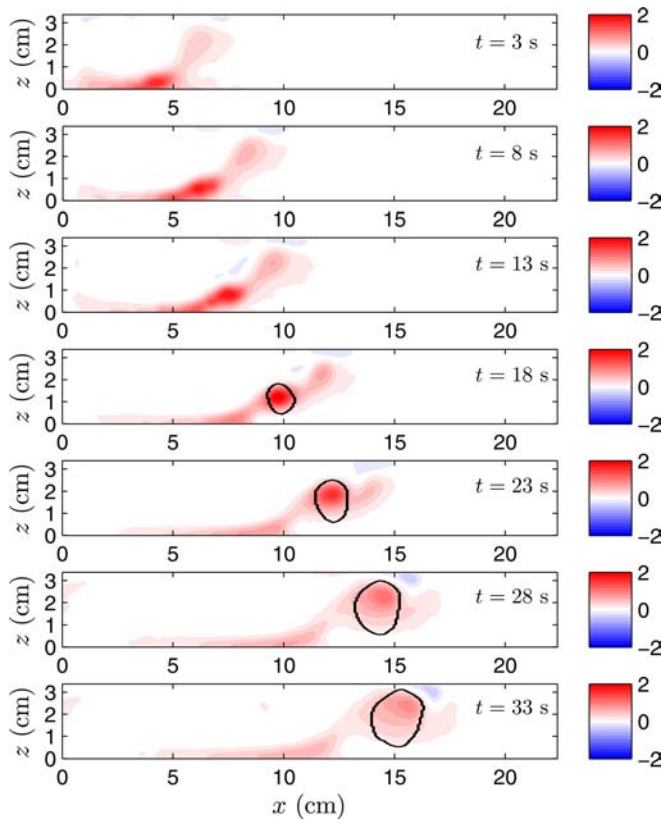
FIG. 5. (Color online) Time evolution of the spanwise vorticity field ω_y (s^{-1}, color/shade) in the vertical symmetry plane for case II ($\alpha = 0.54$, $Re = 290$). The black contour denotes the boundary of the vortex core given by the $\lambda_2 = 0$ isoline.

criterion is a three-dimensional vortex detection method which determines local pressure minima. In particular, this criterion allows a vortex core evolving in a sheared flow to be identified. For the flow considered in this study, it can be shown (see Appendix) that the λ_2-criterion is valid in two dimensions when computed in the vertical symmetry plane of the dipole.

From $t = 3$ s to $t = 23$ s, the spanwise vorticity associated with the viscous boundary layer generated below the propagating dipole is amplified, eventually detaching downstream and progressively rising from the boundary layer at the front of the vortex dipole. At $t = 18$ s, the λ_2-criterion indicates that the initial patch of spanwise vorticity has turned into a spanwise vortex. After $t = 23$ s, the vertical position of the spanwise vortex is quasi constant. During this last stage between $t = 23$ s and $t = 33$ s, the spanwise vortex simply propagates horizontally while increasing in size through diffusion as indicated by the λ_2-criterion.

To interpret the generation of the spanwise vortex, it is helpful to consider the spanwise vorticity equation

$$\frac{\partial \omega_y}{\partial t} + u_x \frac{\partial \omega_y}{\partial x} + u_y \frac{\partial \omega_y}{\partial y} + u_z \frac{\partial \omega_y}{\partial z}$$
$$= \omega_x \frac{\partial u_y}{\partial x} + \omega_y \frac{\partial u_y}{\partial y} + \omega_z \frac{\partial u_y}{\partial z} + \nu \nabla^2 \omega_y, \tag{1}$$

where $\mathbf{u} = (u_x, u_y, u_z)$ and $\boldsymbol{\omega} = (\omega_x, \omega_y, \omega_z)$ denote the velocity and vorticity fields, respectively. In the vertical symmetry

plane of the dipole ($y = 0$), ω_x, ω_z, and $\frac{\partial \omega_y}{\partial y}$ vanish by symmetry. Moreover, since the flow is expected to be quasi-parallel initially because of the vertical invariance of the generation process, the vertical component of the velocity can be neglected initially. Then, at initial time, Eq. (1) reduces to

$$\frac{\partial \omega_y}{\partial t} + u_x \frac{\partial \omega_y}{\partial x} = \omega_y \frac{\partial u_y}{\partial y} + \nu \nabla^2 \omega_y. \tag{2}$$

Thus, whenever there exists a source of spanwise vorticity $\omega_y \neq 0$ in a positive spanwise gradient of the spanwise velocity, $\frac{\partial u_y}{\partial y}$, the stretching term $\omega_y \frac{\partial u_y}{\partial y}$ leads to the amplification of the spanwise vorticity ω_y.

In the present case, the initial source of spanwise vorticity lies in the viscous boundary layer generated at the solid bottom by the propagating dipole. The positive stretching in the spanwise direction can be inferred by the outgoing sectional streamlines at the saddle point at the front of the dipole in Figs. 2(a) and 2(b). This stretching combines with the existing spanwise boundary-layer vorticity and generates the source term for the amplification of spanwise vorticity. Such an amplification locally modifies the flow and eventually leads to the generation of vertical velocity u_z in the vertical symmetry plane. This model of amplification of spanwise vorticity in the viscous boundary layer is in agreement with the results of Fig. 5 which show that the maximum value of the vorticity initially increases until $t \approx 18$ s. (It should also be noted that a patch of low intensity spanwise vorticity above the spanwise vortex can be observed in Fig. 5 at all times. This low intensity patch of spanwise vorticity results from the stretching of noise present initially in the water tank.)

The time for the generation of a mature spanwise vortex, as detected by the λ_2-criterion, can be estimated from the present set of experiments for different Reynolds numbers and aspect ratios α. Table I shows the uncertainty intervals of the time t_{SV} of the spanwise vortex appearance for the three cases (I, II, and III). There exists an overlap between the three cases for the value of the non-dimensional time of spanwise vortex appearance around $t_{SV}/(D_0/U_0) = 0.83$. The overlap and its value close to 1 indicate that the generation of the spanwise vortex scales on the advection time of the dipole.

It can also be concluded from Fig. 5 that the spanwise vortex vorticity can be traced back to a maximum of spanwise vorticity in the viscous boundary layer. The spanwise vorticity extremum allows the spanwise vortex to be identified even in its premature form, before it is detected by the λ_2-criterion. Indeed, it should be noted that in practice, the λ_2-field can be quite noisy and moreover we found that a detection criterion based solely on λ_2 can lead to erroneous identification of vortices. The λ_2-criterion to identify the spanwise vortex was therefore supplemented by the identification of a vorticity maximum.

B. Streamwise trajectories

In this section, the evolution of the streamwise positions of the vortex dipole and of the spanwise vortex is examined.

TABLE I. Uncertainty intervals of the time t_{SV} of the spanwise vortex appearance and $t_{SV}/(D_0/U_0)$ for the three cases I ($Re = 290$, $\alpha = 0.3$), II ($Re = 290$, $\alpha = 0.54$), and III ($Re = 180$, $\alpha = 0.54$).

Case	I	II	III
t_{SV} (s)	[6.5, 12]	[12, 18]	[19, 31]
$t_{SV}/(D_0/U_0)$	[0.45, 0.83]	[0.83, 1.25]	[0.81, 1.32]

The main objective is to identify the relevant timescales of the dominant processes controlling the time evolution of the vortex dipole and its spanwise vortex.

To this end, in addition to identifying the spanwise vortex in the vertical symmetry plane as in Sec. IV, it is necessary to determine the position of the vortex dipole from the available vertical plane measurements. The center of an ideal two-dimensional dipole can be identified by the position of the maximum streamwise velocity on the axis of symmetry. In the present case of a shallow dipole with vertical gradients, the streamwise position of the dipole center was therefore determined by the position of the maximum of streamwise velocity averaged over the water depth. It has been verified by comparisons of all available data in horizontal planes that the streamwise position of the vortex dipole is well determined by this technique.

Figures 6(a) and 6(b) present the horizontal trajectories of the vortex dipole (full symbols) and the spanwise vortex (empty symbols) for the three cases I, II, and III in dimensional and non-dimensional forms, respectively. In Fig. 6(a), it can be seen that for both the vortex dipole and the spanwise vortex, the influence of the aspect ratio is negligible, whereas the Reynolds number radically affects the trajectories. In Fig. 6(b), the streamwise positions have been non-dimensionalized by the characteristic horizontal lengthscale D_0 and time has been non-dimensionalized by the advective timescale D_0/U_0. For the dipole as well as for the spanwise vortex, the trajectories collapse for all values of the aspect ratio and the Reynolds number. The dipole advective timescale D_0/U_0 (which is equivalent to the flap closing time T_c) thus controls the streamwise propagation of both structures. Yet, the non-dimensional trajectories of the two structures differ and diverge with time, the spanwise vortex moving faster than the primary vortices.

C. Vertical trajectories of the spanwise vortex

Figures 7(a)–7(c) describe the time evolution of the vertical position of the spanwise vortex dimensionally and with two different non-dimensionalizations, respectively, for the three cases I, II, and III. Figure 7(a) shows the dimensional vertical trajectories of the spanwise vortex as a function of time. The trajectories are composed of two stages, a rising one for early times after the closing of the flaps and a "hovering" stage for later times. Between both, the spanwise vortex reaches a maximum height which depends strongly on confinement: case I for $\alpha = 0.3$ is significantly lower than cases II and III for $\alpha = 0.54$. During the "hovering" stage, the spanwise vortex stays at a quasi constant height but closer examination reveals a slight decrease for all three cases.

In Fig. 7(b), the vertical trajectories of the spanwise vortex have been non-dimensionalized by the viscous boundary layer thickness $\delta = D_0/\sqrt{Re}$. This characteristic length-scale has been chosen rather than h since the spanwise vortex originates from the boundary layer. Time has been non-dimensionalized by the dipole advection timescale D_0/U_0. With this scaling, all trajectories collapse during the early rising stage, until $t \approx D_0/U_0$. This suggests that the boundary-layer thickness is a relevant lengthscale for the short-time dynamics of the spanwise vortex. It also indicates that not only the streamwise propagation [see Fig. 6(b)] but also the initial rising stage of the spanwise vortex takes place on the advection timescale D_0/U_0. In other words, the short-time dynamics of the spanwise vortex depends only on the propagation of the vortex dipole. This stage ends when the spanwise vortex is identified as such by the λ_2-criterion, in addition to a local vorticity maximum which clearly separates the vortex from the viscous boundary-layer. During the late rising stage for $t > D_0/U_0$, the spanwise vortex keeps moving up to reach a maximum height. However, this maximum does not depend on δ, suggesting that another vertical lengthscale controls the dynamics of the spanwise vortex at large times.

Figure 7(c) thus shows the vertical trajectories of the spanwise vortex non-dimensionalized by the water depth h as a function of time non-dimensionalized by the vertical diffusion time-scale h^2/ν. With this new scaling, the different trajectories exhibit the same behavior at large times. The
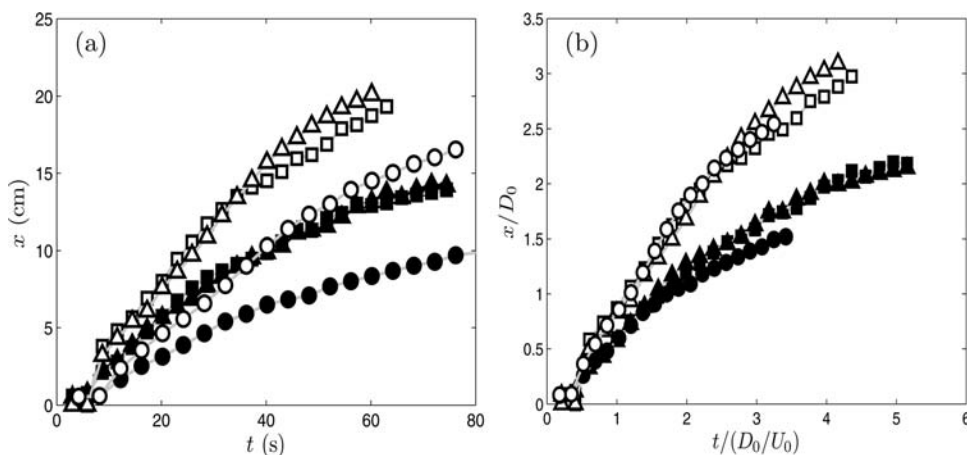

FIG. 6. Time evolution of the streamwise positions of the vortex dipole (full symbols) and the spanwise vortex (empty symbols) in the vertical symmetry plane $y = 0$, for the three flow cases I ($Re = 290$, $\alpha = 0.3$, squares), II ($Re = 290$, $\alpha = 0.54$, triangles), and III ($Re = 180$, $\alpha = 0.54$, circles). Dimensional trajectories $x(t)$ (a) and non-dimensional trajectories x/D_0 as a function of tU_0/D_0 (b).
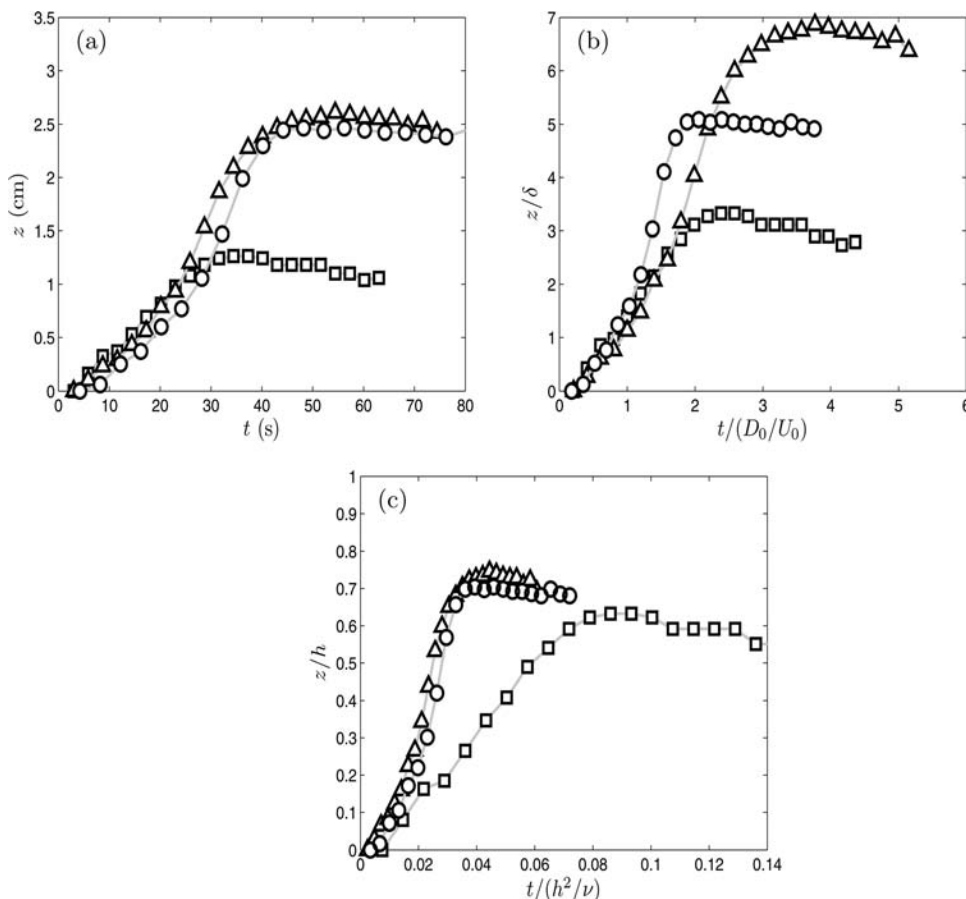
FIG. 7. Time evolution of the vertical position of the spanwise vortex in the vertical symmetry plane $y = 0$ for the three flow cases I ($Re = 290$, $\alpha = 0.3$, squares), II ($Re = 290$, $\alpha = 0.54$, triangles), and III ($Re = 180$, $\alpha = 0.54$, circles). Dimensional trajectories $z(t)$ (a), non-dimensional trajectories z/δ as a function of tU_0/D_0 (b), and non-dimensional trajectories z/h as a function of $t\nu/h^2$ (c). $\delta = D_0/\sqrt{Re}$ corresponds to the boundary-layer thickness.

collapse for all aspect ratios α and Reynolds numbers Re is good when considering that the trajectories follow a common slightly descending trend, after the spanwise vortex has reached its maximum height. This suggests that the water depth h controls the late-time motion of the spanwise vortex on a viscous timescale h^2/ν.

In the intermediate stage, i.e., after the spanwise vortex has detached from the boundary layer and before it reaches its maximum height, the dynamics does not seem to be controlled by a single lengthscale. Moreover, there is a strong influence of the aspect ratio α. Also, it can be noted that the maximum height reached by the spanwise vortex is closer to the free surface than the bottom (i.e., $z/h > 0.5$). This maximum position is followed by a downward drift which can be qualitatively explained by considering the boundary layer developing at the free surface. Indeed, a tangential stress is generated at the free surface and consequently a viscous boundary layer (whose vorticity is of opposite sign compared with the spanwise vortex vorticity) develops as the spanwise vortex rises and approaches the free surface (Fig. 5, $t > 18$ s). Viscous annihilation of vorticity is then induced by cross-diffusion between this free-surface boundary layer and the spanwise vortex. This mechanism erases the vorticity at the top of the spanwise vortex, resulting in the descent of the maximum of spanwise vorticity on a viscous timescale.

D. Vorticity

Figures 8(a)–8(c) describe the time evolution of the maximum spanwise vorticity in the vertical symmetry plane

$y = 0$, associated with the spanwise vortex dimensionally and with two different non-dimensionalizations, respectively, for the three cases I, II, and III.

Figure 8(a) shows the dimensional maximum spanwise vorticity as a function of time. As for the vertical trajectory, two regimes can be identified, at least for cases I and II: a short-time amplification followed by a decay, as observed in Fig. 5. For case III, the vorticity decreases continuously but a plateau can be observed around $t = 30$ s.

In Fig. 8(b), the maximum of spanwise vorticity has been non-dimensionalized by the boundary-layer shear U_0/δ. Time has been non-dimensionalized by the advection timescale D_0/U_0. At short times, the amplitude scales relatively well for cases I and II. Moreover, the peak vorticity is reached at $t \approx D_0/U_0$ for both cases concurrently with the identification of the spanwise vortex by the λ_2-criterion. Case III is qualitatively different and a plateau instead of a peak is observed at this time, which coincides with the emergence of a proper spanwise vortex [see Fig. 7(b)]. The similarities between the three cases confirm that the generation of the spanwise vortex takes place on the advection timescale D_0/U_0 and that its vorticity is well correlated with the boundary-layer vorticity. This validates the previous observation that the source of vorticity for the spanwise vortex is the boundary layer. Moreover, the vorticity measured in the spanwise vortex for cases I and II increases above the boundary layer vorticity level ($\omega_{max} \approx 1.5 U_0/\delta$) which is consistent with the vorticity amplification mechanism *via* spanwise stretching as described in Sec. V A.
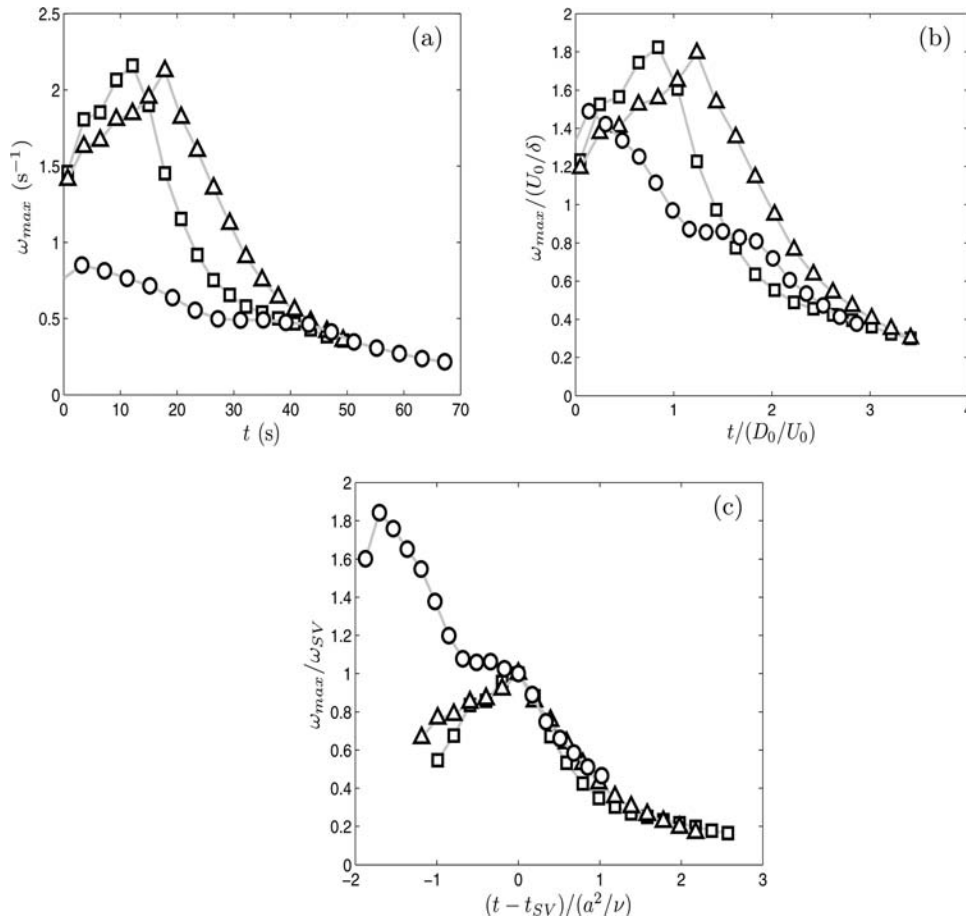
FIG. 8. Time evolution of the spanwise vorticity extremum ω_{max} in the vertical symmetry plane $y = 0$ for the three flow cases I ($Re = 290$, $\alpha = 0.3$, squares), II ($Re = 290$, $\alpha = 0.54$, triangles), and III ($Re = 180$, $\alpha = 0.54$, circles). Dimensional vorticity $\omega_{max}(t)$ (a), non-dimensional vorticity $\omega_{max}/(U_0/\delta)$ as a function of $t/(D/U_0)$ (b), and non-dimensional vorticity ω_{max}/ω_{SV} as a function of $(t - t_{SV})/(a^2/\nu)$ (c), where t_{SV} is the generation time of the spanwise vortex, a its radius, and ω_{SV} its maximum vorticity at t_{SV}.

Once the spanwise vortex is mature and reaches its maximum height, it is expected to experience viscous diffusion at later times. This is confirmed by the results displayed in Fig. 8(c), where the maximum vorticity is rescaled by the maximum vorticity at the time t_{SV} of the spanwise vortex appearance (see Sec. V A) and time is non-dimensionalized by the characteristic diffusion time of the spanwise vortex a^2/ν. Here $a = \sqrt{\nu/(U_0/D_0)}$ is the radius of the spanwise vortex, as discussed in Sec. IV B. The collapse of the three curves with this rescaling suggests that the same process of viscous diffusion dominates the dynamics of the spanwise vortex at this stage in the three cases.

VI. CONCLUSION

The present experimental study of shallow vortex dipoles underlines the relevance of three non-dimensional parameters: the two control parameters $\alpha = h/D_0$ (the aspect ratio) and $Re = U_0 D_0/\nu$ (the Reynolds number), plus the combination $\alpha^2 Re$. For small $\alpha^2 Re$, the flow was observed to remain quasi-parallel, its dynamics being dominated by viscous dissipation in the entire water layer. By contrast, inertia of the vortex dipole becomes dominant for larger values of $\alpha^2 Re$ and allows a spanwise vortex to be generated in the water layer at the front of the dipole for $\alpha^2 Re \gtrsim 6$. However, the early-time dynamics of the spanwise vortex shows very little dependence on $\alpha^2 Re$ and is mainly influenced by the dipole Reynolds number. Indeed, when considering the span-

wise vortex regime for different $\alpha^2 Re$, the same behavior is observed when the Reynolds number is the same whereas a different Reynolds number leads to a qualitatively different early-time behavior. Therefore, the early-time dynamics is controlled by the Reynolds number and does not depend on the aspect ratio α. Moreover, it is shown that the spanwise vortex originates from the boundary layer produced by the propagating dipole over the no-slip, rigid bottom. As the spanwise vorticity detaches from the boundary layer, it is amplified and focused by the spanwise stretching field at the front of the dipole. This mechanism generates a spanwise vortex on an advective timescale D_0/U_0, whose vorticity increases above the levels of vorticity found in the boundary layer. Once the spanwise vortex has separated from the boundary layer, its motion is controlled by the vertical confinement, i.e., the aspect ratio α and its long-term dynamics become dominated by viscous diffusion.

With regard to geophysical applications such as coastal dipoles, for which the aspect ratio can be roughly estimated to $\alpha \sim 0.1$ (Ref. [1]), a typical oceanic turbulent viscosity of 2×10^{-2} m²/s (e.g., Ref. [26]) yields $\alpha^2 Re \sim 7$. Such an estimate is slightly above the critical value found in the present study and therefore suggests that the spanwise vortex regime could be observed in coastal dipoles. It should be noted that Smith and Largier[1] attribute the sediment transport measured in geophysical dipoles to three-dimensional motions in accordance with the motions induced by a spanwise vortex as observed in the present lab experiments.

APPENDIX: THE λ_2-CRITERION IN A SYMMETRY PLANE

The λ_2-criterion is based on the concept that the vorticity-induced pressure is sectionally minimum in a vortex. In a plane, the local pressure reaches a minimum if the pressure gradient is equal to zero and the pressure second-order derivatives along two orthogonal tangent directions are both positive. In order to ensure this condition, Jeong and Hussain[25] proposed a criterion derived from the decomposition of the velocity gradient tensor $\nabla \mathbf{u} = D + \Omega$, where D and Ω are, respectively, the symmetric and antisymmetric parts of $\nabla \mathbf{u}$. A new tensor G can be defined as

$$G = D.D^T - \Omega.\Omega^T.$$

G is symmetric and has real eigenvalues $\lambda_1 \geq \lambda_2 \geq \lambda_3$. It can be shown that the existence of a sectional pressure minimum is ensured by the second eigenvalue of G being negative ($\lambda_2 < 0$).

The λ_2-criterion is thus a three-dimensional criterion and its relevance in the present 2D investigation has to be confirmed. In particular, the eigenvalue associated with the third dimension has to be compared with the other two.

In a symmetry plane such as the vertical symmetry plane (x, z) of the vortex dipole, the spanwise component of the velocity u_y is zero. Moreover, it can be shown that $\partial u_y/\partial x = \partial u_y/\partial z = 0$, $\partial u_y/\partial y \neq 0$, and $\partial u_x/\partial y = \partial u_z/\partial y = 0$.

Then the velocity gradient tensor can be written as

$$\nabla \mathbf{u} = \begin{pmatrix} \dfrac{\partial u_x}{\partial x} & 0 & \dfrac{\partial u_x}{\partial z} \\ 0 & \dfrac{\partial u_y}{\partial y} & 0 \\ \dfrac{\partial u_z}{\partial x} & 0 & \dfrac{\partial u_z}{\partial z} \end{pmatrix}.$$

The symmetric part D of the velocity gradient tensor is

$$D = \frac{1}{2}\begin{pmatrix} 2\dfrac{\partial u_x}{\partial x} & 0 & \dfrac{\partial u_x}{\partial z} + \dfrac{\partial u_z}{\partial x} \\ 0 & 2\dfrac{\partial u_y}{\partial y} & 0 \\ \dfrac{\partial u_x}{\partial z} + \dfrac{\partial u_z}{\partial x} & 0 & 2\dfrac{\partial u_z}{\partial z} \end{pmatrix}.$$

The antisymmetric part Ω of the velocity gradient tensor is

$$\Omega = \frac{1}{2}\begin{pmatrix} 0 & 0 & \dfrac{\partial u_x}{\partial z} - \dfrac{\partial u_z}{\partial x} \\ 0 & 0 & 0 \\ -\dfrac{\partial u_x}{\partial z} + \dfrac{\partial u_z}{\partial x} & 0 & 0 \end{pmatrix}.$$

Thus $G = D.D^T - \Omega.\Omega^T$ has the following expression:

$$G = \begin{pmatrix} \left(\dfrac{\partial u_x}{\partial x}\right)^2 + \dfrac{\partial u_x}{\partial z}\dfrac{\partial u_z}{\partial x} & 0 & \dfrac{1}{2}\left(\dfrac{\partial u_x}{\partial x} + \dfrac{\partial u_z}{\partial z}\right)\left(\dfrac{\partial u_x}{\partial z} + \dfrac{\partial u_z}{\partial x}\right) \\ 0 & \left(\dfrac{\partial u_y}{\partial y}\right)^2 & 0 \\ \dfrac{1}{2}\left(\dfrac{\partial u_x}{\partial x} + \dfrac{\partial u_z}{\partial z}\right)\left(\dfrac{\partial u_x}{\partial z} + \dfrac{\partial u_z}{\partial x}\right) & 0 & \left(\dfrac{\partial u_z}{\partial z}\right)^2 + \dfrac{\partial u_x}{\partial z}\dfrac{\partial u_z}{\partial x} \end{pmatrix}.$$

It then follows that

$$\left| D^2 - \Omega^2 - \lambda I \right| = \left[\left(\dfrac{\partial u_y}{\partial y}\right)^2 - \lambda\right] M_{2D},$$

where I is the identity matrix and

$$M_{2D} = \begin{vmatrix} \left(\dfrac{\partial u_x}{\partial x}\right)^2 + \dfrac{\partial u_x}{\partial z}\dfrac{\partial u_z}{\partial x} - \lambda & \dfrac{1}{2}\left(\dfrac{\partial u_x}{\partial x} + \dfrac{\partial u_z}{\partial z}\right)\left(\dfrac{\partial u_x}{\partial z} + \dfrac{\partial u_z}{\partial x}\right) \\ \dfrac{1}{2}\left(\dfrac{\partial u_x}{\partial x} + \dfrac{\partial u_z}{\partial z}\right)\left(\dfrac{\partial u_x}{\partial z} + \dfrac{\partial u_z}{\partial x}\right) & \left(\dfrac{\partial u_z}{\partial z}\right)^2 + \dfrac{\partial u_x}{\partial z}\dfrac{\partial u_z}{\partial x} - \lambda \end{vmatrix}$$

is a tensor that only needs the velocity field in the (x, z) symmetry plane to be computed. The eigenvalue λ associated with the term $[(\partial u_y/\partial y)^2 - \lambda]$ is necessarily positive. The λ_2-criterion can then be applied in the vertical symmetry plane since the presence of a vortex now only depends on the sign of the largest eigenvalue of the tensor M_{2D}.

[1] J. A. Smith and J. L. Largier, "Observations of nearshore circulations: Rip currents," J. Geophys. Res. **100**, 10967, doi:10.1029/95JC00751 (1995).

[2] M. Gacic, V. Kovacevic, S. Cosoli, A. Mazzoldi, J. D. Paduan, I. Mancero-Mosquera, and S. Yari, "Surface current patterns in front of the Venice Lagoon," Estuarine Coastal Shelf Sci. **82**, 485 (2009).

[3] K. Ahlnas, T. C. Royer, and T. M. George, "Multiple dipole eddies in the Alaska Coastal Current detected with lands at thematic Mapper data," J. Geophys. Res. **92**, 13041, doi:10.1029/JC092iC12p13041 (1987).

[4] S. I. Voropayev, Y. D. Afanasyev, and I. A. Filipov, "Horizontal jets and vortex dipoles in a stratified fluid," J. Fluid Mech. **227**, 543 (1991).

[5] J. B. Flòr and G. J. F. Van Heijst, "An experimental study of dipolar vortex structures in a stratified fluid," J. Fluid Mech. **279**, 101 (1994).

[6] J. B. Flòr, G. J. F. Van Heijst, and R. Delfos, "Decay of dipolar vortex structures in a stratified fluid," Phys. Fluids **7**, 374 (1995).

[7] M. Bonnier, P. Bonneton, and O. Eiff, "Far-wake of a sphere in a stably stratified fluid: Characterization of the vortex structures," Appl. Sci. Res. **59**, 269 (1998).

[8] O. Praud and A. M. Fincham, "The structure and dynamics of dipolar vortices in a stratified fluid," J. Fluid Mech. **544**, 1 (2005).

[9] G. H. Jirka, "Large scale flow structures and mixing processes in shallow flows," J. Hydraul. Res. **39**, 567 (2001).

[10] D. Rockwell, "Vortex formation in shallow flows," Phys. Fluids **20**, 031303 (2008).

[11] D. Sous, N. Bonneton, and J. Sommeria, "Turbulent vortex dipoles in a shallow water layer," Phys. Fluids **16**, 2886 (2004).

[12]D. Sous, N. Bonneton, and J. Sommeria, "Transition from deep to shallow water layer: Formation of vortex dipoles," Eur. J. Mech. B/Fluids **24**, 19 (2005).

[13]M. P. Satijn, A. W. Cense, R. Verzicco, H. J. H. Clercx, and G. J. F. van Heijst, "Three-dimensional structure and decay properties of vortices in shallow fluid layers," Phys. Fluids **13**, 1932 (2001).

[14]J. C. Lin, M. Ozgoren, and D. Rockwell, "Space-time development of the onset of a shallow-water vortex," J. Fluid. Mech. **485**, 33 (2003).

[15]R. A. D. Akkermans, L. P. J. Kamp, H. J. H. Clercx, and G. J. F. Van Heijst, "Intrinsic three dimensionality in electromagnetically driven shallow flows," Europhys. Lett. **83**, 24001 (2008).

[16]R. A. D. Akkermans, A. R. Cieslik, L. P. J. Kamp, R. R. Trieling, H. J. H. Clercx, and G. J. F. Van Heijst, "The three dimensional structure of an electromagnetically generated dipolar vortex in a shallow fluid layer," Phys. Fluids **20**, 116601 (2008).

[17]R. A. D. Akkermans, L. P. J. Kamp, H. J. H. Clercx, and G. J. F. Van Heijst, "Three-dimensional flow in electromagnetically driven shallow two-layer fluids," Phys. Rev. E **82**, 026314 (2010).

[18]L. Lacaze, P. Brancher, O. Eiff, and L. Labat, "Experimental characterization of the 3D dynamics of a laminar shallow vortex dipole," Exp. Fluids **48**, 225 (2009).

[19]M. Duran-Matute, J. Albagnac, L. P. J. Kamp, and G. J. F. Van Heijst, "Dynamics and structure of decaying shallow dipolar vortices," Phys. Fluids **22**, 116606 (2010).

[20]M. Duran-Matute, L. P. J. Kamp, R. R. Trieling, and G. J. F. Van Heijst, "Scaling of decaying shallow axisymmetric swirl flows," J. Fluid Mech. **648**, 471 (2010).

[21]P. Billant and J. M. Chomaz, "Experimental evidence for a new instability of a vertical columnar vortex pair in a strongly stratified fluid," J. Fluid Mech. **418**, 167 (2000).

[22]A. Fincham and G. R. Spedding, "Low cost, high resolution DPIV for measurements of turbulent fluid flow," Exp. Fluids **23**, 449 (1997).

[23]A. Fincham and G. Delerce, "Advanced optimization of correlation imaging velocimetry algorithms," Exp. Fluids **7**(Suppl.), S13 (2000).

[24]J. C. R. Hunt, "Vorticity and vortex dynamics in complex turbulent flows," Trans. Can. Soc. Mech. Eng. **11**, 21 (1987).

[25]J. Jeong and F. Hussain, "On the identification of a vortex," J. Fluid. Mech. **285**, 69 (1995).

[26]M. G. McPhee, *Air-Ice-Ocean Interaction: Turbulent Ocean Boundary Layer Exchange Processes* (Springer, New York, 2008).